ELSEVIER

Journal of Power Sources 75 (1998) 56–63

JOURNAL OF POWER SOURCES

Determination of the hydrogen diffusion coefficient in metal hydrides by impedance spectroscopy

Bala S. Haran *, Branko N. Popov, Ralph E. White

Department of Chemical Engineering, University of South Carolina, Columbia, SC 29208, USA

Received 17 February 1998; accepted 30 March 1998

Abstract

Cobalt coatings on metal hydrides give rise to an additional capacity due to the cobalt on the surface of the alloy. In such a case, the galvanostatic discharge technique cannot be used to measure the diffusion coefficient of hydrogen in the alloy. We present here an analytical impedance model of the metal hydride electrode. This simple model is used to calculate the diffusion coefficient of hydrogen in the metal alloy. The impedance response of cobalt microencapsulated $LaNi_{4.27}Sn_{0.24}$ electrode was measured at different hydrogen contents. From the slope of the Nyquist plot in the transition region the diffusion coefficient of hydrogen was calculated at various states of charge (SOC). It is seen that the diffusion coefficient increases with the hydrogen content in the alloy. The technique applied for cobalt encapsulated $LaNi_{4.27}Sn_{0.24}$ could however be used for any hydrogen storage alloy.

Keywords: Metal hydrides; Impedance; Mathematical modelling; Diffusion; Cobalt compounds

1. Introduction

Many different multi-component AB_5 alloys have replaced cadmium as the negative electrode for alkaline nickel–cadmium batteries [1]. These alloys, commonly known as metal hydrides (MH), store hydrogen as the active material for charge–discharge cycling. The controlling role that the hydrogen diffusion process may have on the hydride electrode's behavior, as opposed to that of the reactions taking place on the alloy surface, is an important factor to consider in determining the kinetic parameters of the MH electrode. In most cases, the performance of the electrode is in mixed control (i.e., neither kinetically controlled nor diffusion controlled alone) [2]. The role of the diffusion coefficient of hydrogen in the alloy assumes significance in such a context.

A wide range of values of the diffusion coefficient has been reported in literature [3–15]. Nuclear magnetic resonance (NMR) [3–6], quasielastic neutron scattering (QNS) [7–10] and electrochemical techniques [11–15] have been used to determine the diffusion coefficient. Using NMR, Karlicek and Lowe [3] found the existence of two different activation energies controlling hydrogen diffusion in β-$LaNi_5$ hydride. They proposed a diffusion mechanism involving two types of hydrogen motion arising from the movement of hydrogen between several potential energy wells of different depths. Bowman, Jr. et al. [4] varied the Al content in β-$LaNi_{5-y}Al_yH_x$ and found that the diffusion coefficient decreased with decrease in hydrogen content in the alloy. Increased Al substitutions was found to significantly increase the hydrogen diffusion activation energy and reduce the diffusion coefficient of $LaNi_{3.8}Al_{1.2}H_{4.0}$ by more than two orders of magnitude relative to $LaNi_5H_{6.2}$. Using QNS, Richter and Hemplemann [7] observed a slow motion (jump diffusion) in addition to an obviously rapid motion, suggesting that there are at least two types of hydrogen motion with different time scales. Also, they found a concentration dependence with the diffusion coefficient increasing with increasing hydrogen content. With neutron scattering Noreus et al. [8] measured the H-diffusion coefficient at various temperatures. Adopting a similar technique, Lebsanft et al. [9] measured the temperature dependence of hydrogen mobility in a variety of MH systems. Fischer et al. [10] used inelastic neutron scattering to provide information regarding the dynamics of hydrogen in $LaNi_5H_x$ by correlating the data qualitatively to a jump diffusion model. Zuchner et al. [11] used a current pulse method to

* Corresponding author.

0378-7753/98/$19.00
PII S0378-7753(98)00092-5

determine the diffusion of hydrogen in $LaNi_5$ single crystals as a function of crystal orientation and temperature. Ciureanu et al. [13] made electrochemical studies on $Ni_{64}Zr_{36}$ and determined the diffusion coefficient of hydrogen using the chronopotentiometric method. They found a strong dependence of the diffusion coefficient on the hydrogen concentration. The values increased from 2.2×10^{-14} m^2/s to 4.5×10^{-14} m^2/s for H/M ratios of 2.65 to 6.36, respectively.

Zheng et al. [14] estimated the diffusion coefficient of hydrogen through a palladium plated $LaNi_{4.25}Al_{0.75}$ electrode using constant current and constant potential discharge techniques and reported values of 3.3×10^{-11} and 2.97×10^{-11} cm^2/s, respectively. With the same constant current discharge technique, Zheng et al. [15] determined the diffusion coefficient of hydrogen in copper plated and bare $LaNi_{4.27}Sn_{0.24}$ alloy. The technique consists of measuring the discharge curve of the hydride electrode under a low constant current. In such a case, the discharge remains under kinetic and diffusion control during most part with no ohmic limitations. For a constant flux at the surface and uniform initial concentration of hydrogen in the alloy, the value of the diffusion coefficient was found mathematically for large discharge times [14],

$$\frac{D}{R^2} = \frac{1}{15\left(\frac{Q_o}{j} - \tau\right)}. \quad (1)$$

The transient time given by τ corresponds to the total time taken for the electrode potential to reach -0.6 V vs. Hg/HgO at the given discharge rate. At the end of discharge the surface hydrogen concentration of the alloy particle approaches values close to zero. The ratio Q_o/j corresponds to the time necessary to completely discharge the electrode under hypothetical conditions when the process proceeds without any kinetic and diffusional limitations. Hence the ratio of the diffusion coefficient of hydrogen to the square of the particle radius is inversely proportional to the amount of hydrogen $(Q_o/j - \tau)$ in the electrode after discharge. The derivation in this case is based on the fact that the hydrogen desorption reaction is the only faradaic reaction involved during the entire discharge of the electrode. However, this is not true in all cases. The effect of cobalt microencapsulation on the performance of the hydride alloys has been investigated recently [16]. Discharge profiles of the cobalt encapsulated $LaNi_{4.27}Sn_{0.24}$ reveal two different discharge curves as shown in Fig. 1. The additional curve arises because of the faradaic reaction of cobalt at the surface of the particle [16]. The increase in capacity due to the cobalt coating has also been observed when mixing cobalt powders [17,18], or cobalt oxide [19] with the alloy. In such cases the diffusion coefficient cannot be determined by the technique outlined above. Arriving at an analytical solution when two different faradaic reactions are involved at the surface would be rigorous and complicated. We propose here a simple method based on impedance techniques for the determination of diffusion coefficient in hydride alloys. Motupally et al. [20] used electrochemical impedance spectroscopy (EIS) to measure the solid-state diffusion coefficient of protons in nickel hydroxide films as a function of state of charge. This model of planar diffusion of protons is extended to spherical coordinates and is used to determine the diffusion coefficient of hydrogen in MH. Although, the specific purpose is to determine the diffusion coefficient in cobalt encapsulated $LaNi_{4.27}Sn_{0.24}$, the technique could be used for any hydrogen storage alloy.

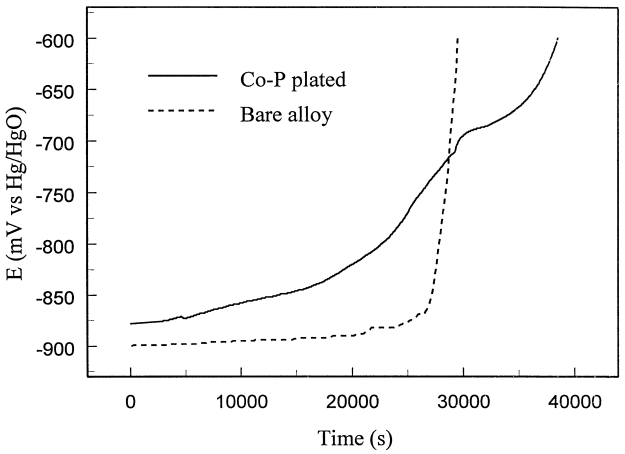

Fig. 1. Discharge curve of the cobalt microencapsulated $LaNi_{4.27}Sn_{0.24}$ electrode. The additional faradaic capacity arises due to the cobalt coating on the surface. The discharge curve for the bare alloy is also given for comparison.

2. Model development

The MH electrode shown in Fig. 2 is modeled in this work. The cylindrical hydride electrode is filled with spherical alloy particles that are in close contact with each other. We consider here a single hydride particle and model the reaction and diffusion in such a case. The ohmic polarization due to changes in the concentration of electrolyte and the particle to particle contact resistance has not been considered. The electrode reaction at the surface of the hydride particle is,

$$MH_{x,ads} + xOH^- \underset{\text{charge}}{\overset{\text{discharge}}{\Leftrightarrow}} M + xH_2O + xe^-. \quad (2)$$

Since ohmic losses are neglected, the current at the interface due to reaction (2) depends on the hydrogen concentration at the surface, c_s and also on the surface overpotential, η_s. Considering the diffusion of hydrogen in spherical coordinates we have [2],

$$\frac{\partial c}{\partial t} = \frac{D}{r^2}\left(r^2 \frac{\partial c}{\partial r}\right) \quad (3)$$

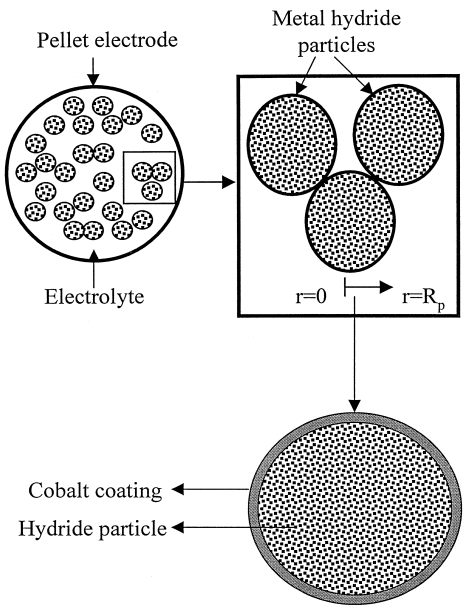

Fig. 2. Schematic of the spherical hydride particles immersed in 6 M KOH solution. The electrochemical reaction takes place at the surface of the particle at $r = R$. Hydrogen diffuses to the bulk of the material during charge. The cobalt coating on the surface of the particle gives the additional faradaic curve seen in Fig. 1.

where D is the hydrogen diffusion coefficient in the alloy. Initially, the concentration of hydrogen in the particle is the same throughout

$$\text{at } t = 0,\ c = c^{o}. \tag{4}$$

The boundary conditions are given by:

$$\text{at } r = 0,\ \frac{\partial c}{\partial r} = 0 \tag{5}$$

$$\text{at } r = R,\ D\frac{\partial c}{\partial r} = -\frac{j'}{F} \tag{6}$$

where the first boundary condition denotes symmetry at the center of the particle while the second one equates the flux of hydrogen at the surface to the reaction rate. The local current density, j', represents the reaction rate at the particle/solution interface. This is related to the current per unit mass of the electrode, j expressed in A/g applied to the current collector, through the amount of material, w_{MH}, volume of the pellet, V, electrode porosity, ε, and the electroactive surface area per unit volume of the electrode, a_{MH}.

$$j' = \frac{jw_{MH}}{a_{MH}V(1-\varepsilon)}. \tag{7}$$

Taking Laplace transforms of Eqs. (3)–(6) with respect to t and then solving the resulting ordinary differential equations we have,

$$\bar{c} = \frac{c^{o}}{p} - \frac{1}{r}\frac{\bar{j}w_{MH}R^{2}}{a_{MH}V(1-\varepsilon)FD} \times \frac{\sinh\left(\sqrt{\frac{p}{D}}\,r\right)}{\sqrt{\frac{pR^{2}}{D}}\cosh\left(\sqrt{\frac{pR^{2}}{D}}\right) - \sinh\left(\sqrt{\frac{pR^{2}}{D}}\right)} \tag{8}$$

where the overbar indicates variables in the Laplace domain. The surface concentration is obtained as,

$$\bar{c}_{s} = \frac{c^{o}}{p} - \frac{\bar{j}w_{MH}R}{a_{MH}V(1-\varepsilon)FD} \times \frac{\sinh\left(\sqrt{\frac{pR^{2}}{D}}\right)}{\sqrt{\frac{pR^{2}}{D}}\cosh\left(\sqrt{\frac{pR^{2}}{D}}\right) - \sinh\left(\sqrt{\frac{pR^{2}}{D}}\right)}. \tag{9}$$

The faradaic impedance of an electrochemical system is defined as

$$Z = \frac{\mathrm{d}\eta}{\mathrm{d}j} \tag{10}$$

where η is the reaction overpotential and j is the resulting current due to reaction (2). At the interface, the total differential of the current due to reaction (2) can be written as,

$$\mathrm{d}j = \frac{\partial j}{\partial c_{s}}\mathrm{d}c_{s} + \frac{\mathrm{d}j}{\mathrm{d}\eta_{s}}\mathrm{d}\eta_{s}. \tag{11}$$

Substituting Eq. (11) into Eq. (10) and converting the resulting equation to the Laplace domain we have,

$$\bar{Z} = \frac{\mathrm{d}\bar{\eta}_{s}}{\left[\left(\frac{\partial\bar{j}}{\partial\bar{c}_{s}}\right)\mathrm{d}\bar{c}_{s} + \left(\frac{\partial\bar{j}}{\partial\bar{\eta}_{s}}\right)\mathrm{d}\bar{\eta}_{s}\right]}. \tag{12}$$

Simplifying Eq. (12) we have,

$$\bar{Z} = \left[\frac{\partial\bar{j}}{\partial\bar{c}_{s}}\left(\frac{\mathrm{d}\bar{c}_{s}}{\mathrm{d}\bar{\eta}_{s}}\right) + \frac{\partial\bar{j}}{\partial\bar{\eta}_{s}}\right]. \tag{13}$$

The differential of the concentration with respect to the overpotential, $\mathrm{d}\bar{c}_{s}/\mathrm{d}\bar{\eta}_{s}$, is obtained by differentiating the

surface concentration given by Eq. (9) with respect to the overpotential, $\bar{\eta}_s$

$$\frac{d\bar{c}_s}{d\bar{\eta}_s} = -\frac{1}{Z}\frac{w_{MH}R}{a_{MH}V(1-\varepsilon)FD} \times \frac{\sinh\left(\sqrt{\frac{pR^2}{D}}\right)}{\sqrt{\frac{pR^2}{D}}\cosh\left(\sqrt{\frac{pR^2}{D}}\right) - \sinh\left(\sqrt{\frac{pR^2}{D}}\right)}. \quad (14)$$

Substituting Eq. (14) into Eq. (13) we have,

$$\bar{Z} = \frac{\partial\bar{\eta}_s}{\partial\bar{j}} + \frac{\left(\partial\bar{j}/\partial\bar{c}_s\right)}{\left(\partial\bar{j}/\partial\bar{\eta}_s\right)}\left[\frac{w_{MH}R}{a_{MH}V(1-\varepsilon)FD} \times \frac{\sinh\left(\sqrt{\frac{pR^2}{D}}\right)}{\frac{\sqrt{pR^2}}{D}\cosh\left(\sqrt{\frac{pR^2}{D}}\right) - \sinh\left(\sqrt{\frac{pR^2}{D}}\right)}\right]. \quad (15)$$

Eq. (15) needs to be transferred to the frequency domain, in order to analyze the impedance data. Assuming that a small perturbation (<10 mV) does not alter the system from steady state, we could substitute $s = i\omega$ [20] into Eq. (15) where i is the imaginary number $\sqrt{-1}$ and ω is the frequency in radians per second.

$$Z(\omega) = \frac{\partial\bar{\eta}_s}{\partial\bar{j}} + \frac{(1-i)\sigma}{\sqrt{\omega\left[\coth[(1+i)\psi] - \frac{(1-i)}{2\psi}\right]}} \quad (16)$$

where σ (Warburg coefficient) is given by

$$\sigma = \frac{\left(\partial\bar{j}/\partial\bar{c}_s\right)}{\left(\partial\bar{j}/\partial\bar{\eta}_s\right)}\left[\frac{w_{MH}}{a_{MH}V(1-\varepsilon)F\sqrt{2D}}\right] \quad (17)$$

and

$$\psi = \sqrt{\frac{\omega R^2}{2D}}. \quad (18)$$

The first term in Eq. (16) corresponds to the faradaic impedance and the second term gives the diffusion impedance. It can be seen that the reaction resistance does not affect the slope of the total impedance as given by Eq. (16). Separating the diffusion impedance into real (Re) and imaginary (Im) parts we have,

$$Z(\omega) = \mathrm{Re} + i\,\mathrm{Im} \quad (19)$$

where

$$\mathrm{Re} = \frac{\sigma}{\sqrt{\omega}}\left[\frac{(T_1 - T_2)}{(T_1^2 + T_2^2)}\right] \quad (20)$$

$$\mathrm{Im} = -\frac{\sigma}{\sqrt{\omega}}\left[\frac{(T_1 + T_2)}{T_1^2 + T_2^2)}\right] \quad (21)$$

$$T_1 = \frac{\sinh(\psi)\cosh(\psi)}{\sinh(\psi)^2 + \sin(\psi)^2} - \frac{1}{2\psi} \quad (22)$$

$$T_2 = -\frac{\sinh(\psi)\cos(\psi)}{\sinh(\psi)^2 + \sin(\psi)^2} + \frac{1}{2\psi}. \quad (23)$$

Differentiating the Re part (given by Eq. (20)) and the Im part (given by Eq. (21)), we obtain the slope of the diffusion controlled impedance plot,

$$\frac{d(\mathrm{Im})}{d(\mathrm{Re})} = \frac{T_4[-T_3 + (S_3S_5 + S_4S_7 - S_1S_6 + S_2S_8)\psi] - 2T_3(S_4S_3 + S_2S_1)\psi}{T_4[-T_5 + (S_3S_6 + S_4S_8 - S_1S_5 + S_2S_7)\psi] - 2T_5(S_4S_3 + S_2S_1)\psi} \quad (24)$$

where

$$T_3 = (S_4S_5 - S_2S_6); T_4 = (S_4^2 + S_2^2);$$
$$T_3 = (S_4S_6 + S_2S_5) \quad (25)$$

and

$$S_1 = S_5S_6; S_2 = 2\psi - S_5;$$
$$S_3 = 2\coth(\psi)\cot(\psi)(1 - \psi S_6) - 2\psi S_5 + S_8 \quad (26)$$
$$S_4 = 2\psi\coth(\psi)\cot(\psi) - S_6;$$
$$S_5 = \coth(\psi) - \cot(\psi) \quad (27)$$
$$S_6 = \coth(\psi) + \cot(\psi); S_7 = 2 - S_1;$$
$$S_8 = \cot(\psi)^2 + \coth(\psi)^2 \quad (28)$$

Eq. (24) involves only the parameter ψ (given by Eq. (18)) and can be used to extract the diffusion coefficient by equating it to the slope in the transition region [20]. The model simulations and the diffusion coefficient calculations were done using Maple®.

3. Experimental

$LaNi_{4.27}Sn_{0.24}$ alloy was crushed and ground mechanically. The alloy was then plated with 28% (by wt.) of cobalt in an alkaline hypophosphite bath. An electrode was prepared by mixing the alloy with 2.5% w/o PTFE followed by hot pressing the material between two nickel meshes at 300°C and 5 t/cm^2 in a cylindrical press. A pellet of 0.7 cm diameter, 0.60 mm thickness and 450 mg weight was obtained. Characterization studies were done in a three-electrode setup. The working pellet electrode was inserted between two pieces of plexiglass and immersed in

the cell filled with 6 M KOH solution. All potentials are with respect to the Hg/HgO reference electrode. The counter electrode is a nickel electrode. The cell was maintained at a constant temperature of 25°C using a water bath. Bitrode Model LCN automated cycle life tester was used for cycling the electrode. Electrochemical studies were done using the Model 352 SoftCorr System with EG and G Princeton Applied Model 273 potentiostat/galvanostat and a frequency analyzer. After conditioning the electrode, SOC studies were performed to determine the electrode characteristics. The active material was discharged for a fixed amount of time at a constant current. The SOC was determined from the ratio of the time discharged to the time required for complete discharge. Once the alloy was discharged to a particular SOC, the electrode was left on open circuit until a stable potential was observed (typically between 45 to 60 min). After the potential stabilized impedance studies were performed. The impedance data generally covers a frequency range from 0.001 Hz to 100 kHz with an AC voltage signal varying by ± 5 mV, which ensures that the electrode system is under minimum perturbation. The SOC studies were repeated until the electrode was discharged to its cut off potential of -0.6 V.

4. Results and discussion

Transport of hydrogen through the spherical particle is the controlling mechanism for thin hydride electrodes. Hydrogen moves in the alloy by a hopping technique, which can be simplified as a slow diffusion process. The parameters of interest in this context are the diffusion coefficient of hydrogen and the particle radius. Fig. 3 presents the effect of varying the diffusion coefficient on

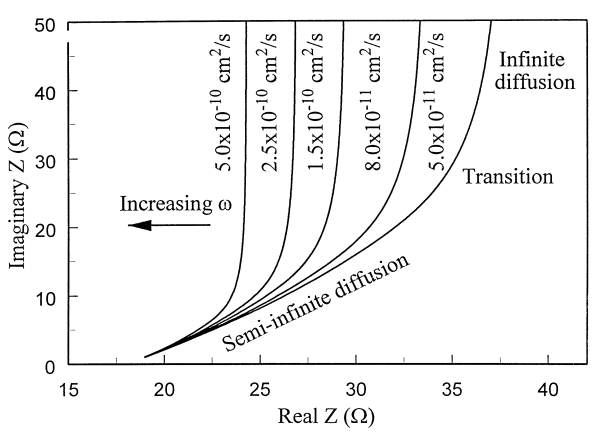

Fig. 3. Nyquist plots of the cobalt-plated electrode simulated for different values of the diffusion coefficient. The semi-infinite diffusion, transition and infinite diffusion regions are shown in the plot. The charge transfer resistance and the Warburg coefficient are fixed as 18 Ω and 1 Ω $s^{-1/2}$, respectively. The average particle size of the alloy was assumed to be 10 μm.

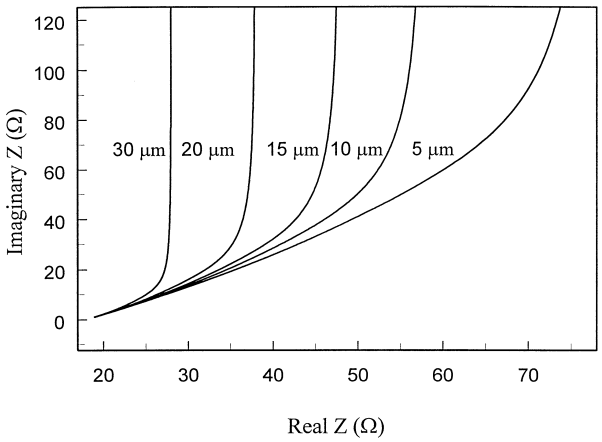

Fig. 4. Change in the Nyquist impedance due to variation in the average particle size of the metal hydride electrode. The simulations were done at a diffusion coefficient value of 2.0×10^{-10} cm^2/s. The charge transfer resistance and Warburg coefficient were set as 18 Ω and 1 Ω $s^{-1/2}$, respectively. Decrease in the particle size or increase in diffusion coefficient (seen in Fig. 4) shifts the onset of the transition region to lower frequencies.

the impedance of the hydride electrode. The charge transfer resistance and the Warburg coefficient have been set to a constant value. In the Nyquist plot, frequency decreases as the real part of the impedance increases. From the plot it can be seen that the impedance response is characterized by three regions namely, semi-infinite diffusion, transition, and finite diffusion regimes. The value of the diffusion coefficient affects not only the magnitude of the impedance but also the transition from semi-infinite to complete diffusion control. As the diffusion coefficient decreases the transition is also shifted to lower frequency values. This is to be expected since lowering the diffusion coefficient reduces the rate of transport of hydrogen across the particle. Since the frequency is inversely proportional to time the transition and diffusion regions appear even later.

Fig. 4 presents the effect of particle size on the Nyquist impedance behavior of the electrode. The plot shows that the effect of particle size is opposite to that of the diffusion coefficient, i.e., decrease in the particle radius shifts the appearance of the transition region to higher frequencies. Since in smaller particles, hydrogen needs to travel only a short distance the time for diffusion is smaller. Hence the diffusion regime appears at higher frequencies. The model simulations indicate that it is desirable to have particles of smaller size. However, as the alloy is cycled it undergoes rapid reduction in particle size. This results due to the volume expansion of the alloy during absorption/desorption of hydrogen. Sakai et al. [21] reported the change in volume by hydrogen absorption for a family of La–Ni alloys. The change in volume ratio varied from 24% for $LaNi_5$ to 14.6% for $LaNi_{2.5}Co_{2.5}$. Decrease in the particle size exposes more amount of the material to the electrolyte leading to increased alloy corrosion. This causes the capacity of the electrode to fade rapidly. Further, other resis-

tances such as the solution resistance, particle–particle contact resistance also increase with cycling. Hence, even if the particle size reduces, these resistances increase the total impedance of the system. The above factors need to be considered while preparing hydride alloys for practical applications.

Nyquist plots of the cobalt plated alloy at 100% and 80% SOC are shown in Fig. 5. The plot is conspicuous by the absence of the transition and diffusion regions. At high SOC the electrode is completely filled with hydrogen and hence no diffusional limitations are seen for the frequency range of 10^5 to 10^{-3} Hz. When the SOC decreases distinct transition and diffusion regions begin to appear. Hence, the diffusion coefficient was determined at SOC values less than 50%.

Fig. 6 presents the Nyquist plots when the transition and diffusion regions are seen clearly. At high frequencies a straight line with an angle of 45° corresponding to the semi-infinite diffusion region is also seen. At low frequencies the slope of the Im vs. Re plot goes to infinity. The transition region lies between these two frequency regimes. As the alloy is progressively depleted of hydrogen, diffusional limitations appear at even lower frequencies. The appearance of the transition region is also shifted to lower frequencies. Motupally et al. [20] observed a shift in the frequency of three orders of magnitude between fully charged and discharged $Ni(OH)_2$ films. In our case the shift in the frequency from 45% to 0% SOC was less than one order of magnitude. The model simulations in Figs. 3 and 4 show that changes in the diffusion coefficient and the particle size may cause this effect. This indicates that either the diffusion coefficient is decreasing or the particle size is increasing during discharge. In a given charge–discharge cycle, the change in the particle size is not significant enough to shift the onset of transition to low frequencies. Furthermore, the lattice volume expands only upon absorption of hydrogen. These factors indicate that the diffusion coefficient of hydrogen in the alloy varies as a function of SOC.

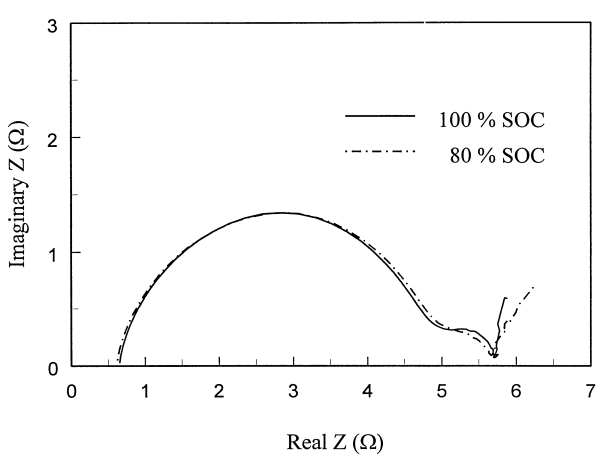

Fig. 5. Experimental Nyquist plots of the cobalt plated alloy at high SOC. Significant diffusional limitations are not seen for the frequency range of 10^{-3} to 10^5 Hz.

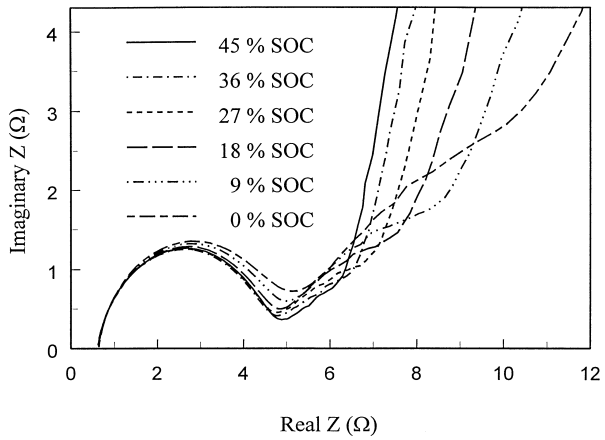

Fig. 6. Experimental Nyquist plots at different hydrogen contents below 50% SOC. The electrode was discharged for a known amount of time to reach a particular SOC. The impedance response was measured once the electrode potential stabilized. The three regions shown in Fig. 3 are seen clearly here. The semicircle at high frequencies arises due to a combination of the double layer at the surface, the polarization resistance and the electrode ohmic resistances.

In literature, impedance data from MH electrodes has in general been fitted to an equivalent circuit and the different cell resistances have been analyzed. Since, our parameter of interest is the diffusion coefficient, the Nyquist plots from Fig. 6 have been re-drawn in Fig. 7 to show only the transition and diffusion limited regions. The shift in the onset of the transition region is seen clearly in these plots. Further, a decrease in the slope with decreasing SOC is also seen. The diffusion coefficient at various SOC was determined by performing a least squares fit of the data to

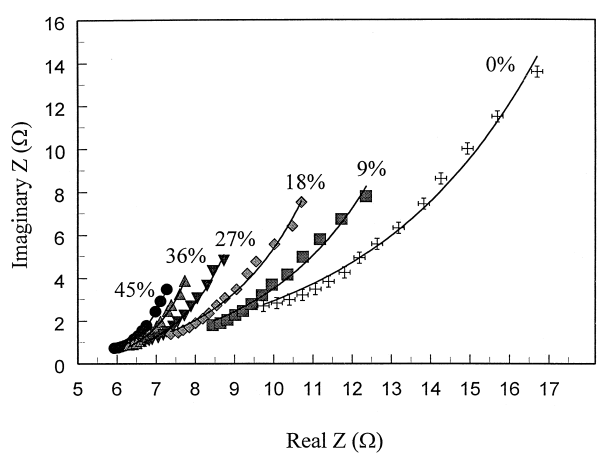

Fig. 7. Nyquist data from Fig. 6 fitted to Eq. (24) at different SOCs. The diffusion coefficient is calculated from the slope of these curves in the transition region. The slope decreases with decrease of hydrogen content in the alloy. For the diffusion coefficient calculations using Eq. (18) the average particle size was taken as 10 μm.

an exponential function as suggested by Motupally et al. [20]

$$\mathrm{Im} = a\,\mathrm{e}^{b\,\mathrm{Re}} \tag{29}$$

where a and b are fitting parameters. Eq. (29) has been used to fit the data shown in Fig. 7. Once the fitting parameters were obtained the function was differentiated at different SOC and the slope was found. This slope is then equated to Eq. (24) and the value of ψ was calculated. The diffusion coefficient was then determined from ψ using Eq. (18).

Fig. 8 presents the diffusion coefficient of hydrogen in cobalt encapsulated $LaNi_{4.27}Sn_{0.24}$ at different SOC. After the electrode is activated the particle size lies in the range of 10–15 μm. Once the value of ψ is known from the slope, the ratio D/R^2 is calculated from Eq. (18). From this ratio, the diffusion coefficient values are determined by taking an average particle size of 10 μm. The diffusion coefficient varies by one order of magnitude between 45% and 0% SOC. A steep decrease is seen at low SOC. The diffusion coefficient varies from 1.671×10^{-10} cm^2/s at 45% SOC to 3.851×10^{-11} cm^2/s at 0% SOC. A similar concentration dependence where the diffusion coefficient increases with hydrogen concentration has been seen previously [4,7,13]. The transport of hydrogen in MH takes place by a hopping mechanism involving two types of hydrogen motion [3,11]. Hydriding of the metal begins with a rapid diffusion of a small amount of H into the interior of the alloy to produce a dilute solid solution denoted as the α-phase [22]. As the hydrogen dissolution proceeds, the α-phase is gradually supersaturated with hydrogen in its surface region and β-hydride starts to deposit [23]. At the end of charging the entire α-solid solution is converted and the alloy particle has hydride in the β-phase [24]. The decrease in the diffusion coefficient at low SOC, could be due to the change in the crystal structure of hydrides when transforming from the α to β phase. The number of vacant sites available for hydrogen to occupy at low SOC is higher as compared to at high SOC. From this it follows that the diffusion coefficient should increase with decrease in SOC. However, the observed trend here and in the previous literature [4,7,13] shows results to the contrary. The model presented in this paper does not allow for definite conclusions about the origin of the observed dependence between D and SOC. While α–β transitions seem to be more critical in determining the role of hydrogen transport, the exact nature and mechanism of hydrogen transport in these two phases is not well known. More solid data is needed before definite conclusions can be drawn.

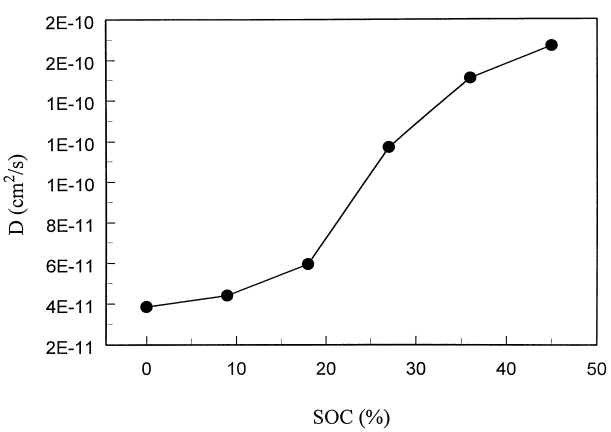

Fig. 8. Diffusion coefficient of hydrogen in the cobalt encapsulated hydride alloy. The diffusion coefficient increases with SOC with an order of magnitude difference between 45% and 0% SOC.

5. Conclusions

A theoretical model for the impedance of metal hydrides has been presented. The model is used to simulate the impedance response of a hydride electrode under diffusional and kinetic limitations. The effect of diffusion coefficient and particle size on the Nyquist plots has also been studied. It is seen that decreasing the diffusion coefficient or increasing the particle size shifts the onset of the transition region to lower frequency values. Impedance data from a cobalt plated $LaNi_{4.27}Sn_{0.24}$ electrode was obtained in the frequency range of 0.001 Hz to 10^5 Hz. The cobalt encapsulation on the surface leads to an additional faradaic capacity giving rise to two discharge curves. Hence, the conventional galvanostatic discharge technique cannot be applied to determine the diffusion coefficient of hydrogen. Nyquist plots of the cobalt-plated electrode reveal three regions at low frequencies namely semi-infinite diffusion, transition, and diffusion limited regimes. The diffusion coefficient was calculated from the slope of the Nyquist plots in the transition region. The technique outlined here is general in nature and could be applied for any MH alloy. It is seen that the diffusion coefficient increases with an increase in the concentration of hydrogen in the particles. A plausible mechanism for the decrease in diffusion coefficient with SOC could be the transformation from the β-phase to the α-phase at low SOC.

6. List of symbols

a_{MH}	electroactive surface area per unit volume of electrode (cm^2/cm^3)
c	concentration of hydrogen (mol/cm^3)
c^o	reference hydrogen concentration (mol/cm^3)
D	diffusion coefficient of hydrogen (cm^2/s)
F	Faraday's constant (96,487 C/mol)
i	imaginary number ($\sqrt{-1}$)
j	specific discharge current (A/g of active material)
j'	microkinetic current density (A/cm^2)
p	Laplace operator (s^{-1})

Q_o specific capacity of the electrode (A · h/g of active material)
r radial coordinate (cm)
R radius of the MH particles (cm)
t time (s)
V volume of the cylindrical pellet electrode (cm^3)
Z total impedance (Ω)
w_{MH} amount of active material (g)

Greek

ε porosity of the electrode
η overpotential (V)
σ Warburg coefficient ($\Omega/s^{1/2}$)
τ total time for discharge (s)
ω frequency (radians/s)
ψ dimensionless parameter $\psi = \dfrac{\sqrt{\omega R^2}}{2D}$

Subscripts

s at the particle–electrolyte interface

Acknowledgements

Financial support by the Exploratory Technology Research (ETR) Program, which is supported by the Office of Transportation Technologies (OTT) of the U.S. Department of Energy (DOE), Subcontract No. 4614610 is acknowledged gratefully.

References

[1] G. Sandrock, in: P.D. Bennett, T. Sakai, (Eds.), Proceedings of the Symposium on Hydrogen and Metal Hydride Batteries, PV 94-27, The Electrochemical Society Proceedings Series, Pennington, NJ 1994, p. 219.
[2] B.S. Haran, B.N. Popov, R.E. White, Theoretical analysis of metal hydride electrodes: studies on equilibrium potential and exchange current density, submitted to J. Electrochem. Soc., December 1997.
[3] R.F. Karlicek Jr., I.J. Lowe, J. Less-Common Met. 73 (1980) 219.
[4] R.C. Bowman Jr., D.M. Gruen, M.H. Mendelsohn, Solid State Commun. 32 (1979) 501.
[5] E. Khodosov, A. Linnik, G. Kobsenko, V. Ivanchenko, Proc. of the 2nd Inter. Congress on Hydrogen in Metals, Paris, paper 1D10, Pergamon, Oxford, 1977.
[6] J.J. Reilly, R.H. Wiswall, Inorg. Chem. 13 (1974) 218.
[7] D. Richter, R. Hemplemann, J. Less-Common Met. 88 (1982) 353.
[8] D. Noreus, L.G. Olsson, U. Dahlborg, Chem. Phys. Lett. 67 (1979) 432.
[9] E. Lebsanft, D. Richter, J.M. Topler, Z. Phys. Chem. N.F. Bd. 116 (1979) 175.
[10] P. Fischer, A. Furrer, G. Busch, L. Schlapbach, Helv. Phys. Acta 50 (1977) 421.
[11] H. Zuchner, T. Rauf, R. Hempelmann, J. Less-Common Met. 172–174 (1991) 611.
[12] M.H.J. Van Rijswick, in: A.F. Anderesen, A.J. Maeland (Eds.), Hydrides for Energy Storage, Pergamon, Oxford, 1981, p. 261.
[13] M. Ciureanu, D.H. Ryan, J.O. Strom-Olsen, M.L. Trudeau, J. Electrochem. Soc. 140 (1993) 579.
[14] G. Zheng, B.N. Popov, R.E. White, J. Electrochem. Soc. 142 (1995) 2695.
[15] G. Zheng, B.N. Popov, R.E. White, J. Electrochem. Soc. 143 (1996) 834.
[16] B.S. Haran, B.N. Popov, R.E. White, submitted to J. Electrochem. Soc., December 1997.
[17] T. Weizhong, G. Yingxin, Z. Haoyu, J. Appl. Electron. 25 (1995) 874.
[18] T. Ikeya, K. Kumai, T. Iwahari, J. Electrochem. Soc. 140 (1993) 3082.
[19] C. Iwakura, Y. Fukumoto, M. Matsuoka, T. Kohno, K. Shinmou, J. Alloys Comp. 192 (1993) 152.
[20] S. Motupally, C.C. Streinz, J.W. Weidner, J. Electrochem. Soc. 142 (1995) 1401.
[21] T. Sakai, K. Oguro, H. Miyamura, N. Kuriyama, A. Kato, H. Ishikawa, J. Less-Common Met. 161 (1990) 193.
[22] X.L. Wang, S. Suda, Int. J. Hyd. Energ. 17 (1992) 139.
[23] C.S. Wang, X.H. Wang, Y.Q. Lei, C.P. Chen, Q.D. Wang, Int. J. Hyd. Energ. 21 (1996) 471.
[24] W. Zhang, S. Srinivasan, H.J. Ploehn, J. Electrochem. Soc. 143 (1996) 4039.